

Brain-ID: Learning Contrast-agnostic Anatomical Representations for Brain Imaging

Peirong Liu¹ Oula Puonti¹ Xiaoling Hu¹
Daniel C. Alexander² Juan E. Iglesias^{1,2}

¹Harvard Medical School and Massachusetts General Hospital ²UCL

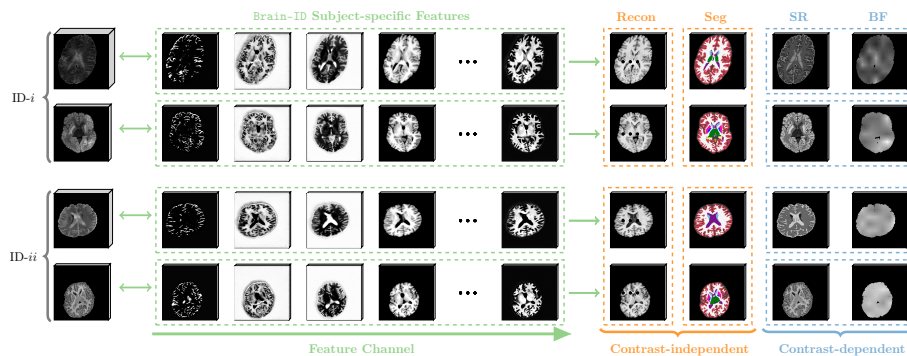


Fig. 1: Brain-ID features serve as the distinctive identity of each subject (ID) regardless of appearance (contrast, deformation, corruptions, etc) and quickly adapt to downstream tasks – either contrast-independent (anatomy **Re**construction, **Seg**mentation), or contrast-dependent (**S**uper-**R**esolution, **B**ias **F**ield estimation), all through one layer.

Abstract. Recent learning-based approaches have made astonishing advances in calibrated medical imaging like computerized tomography (CT), yet they struggle to generalize in uncalibrated modalities – notably magnetic resonance (MR) imaging, where performance is highly sensitive to the differences in MR contrast, resolution, and orientation. This prevents broad applicability to diverse real-world clinical protocols. We introduce **Brain-ID**, an anatomical representation learning model for brain imaging. With the proposed “mild-to-severe” intra-subject generation, **Brain-ID** is robust to the subject-specific brain anatomy regardless of the appearance of acquired images (e.g., contrast, deformation, resolution, artifacts). Trained entirely on synthetic data, **Brain-ID** readily adapts to various downstream tasks through only one layer. We present new metrics to validate the intra- and inter-subject robustness of **Brain-ID** features, and evaluate their performance on four downstream applications, covering contrast-independent (anatomy reconstruction/contrast synthesis, brain segmentation), and contrast-dependent (super-resolution, bias field estimation) tasks (Fig. 1). Extensive experiments on six public datasets demonstrate that **Brain-ID** achieves state-of-the-art performance in all tasks on different MRI modalities and CT, and more importantly, preserves its performance on low-resolution and small datasets. Code is available at <https://github.com/peirong26/Brain-ID>.

1 Introduction

Magnetic resonance imaging (MRI) enables in vivo noninvasive imaging of the human brain with exquisite and tunable soft-tissue contrast [7]. Recent machine learning based methods have achieved great improvements in faster and more accurate image analysis of brain MRI [26], such as image segmentation [17, 31, 40, 45], registration [3, 47, 53, 61], super-resolution [50, 51], and connectivity studies [43]. However, most existing MRI analysis methods are specific to certain MR contrast(s) and often require near-isotropic acquisitions. Therefore, models face sharp performance drops when voxel size and anisotropy increase, or are being used for a different contrast than what seen during training [55]. This reduces model generalizability and results in duplicate data collection and training efforts given new datasets. By resorting to synthetic data, recent contrast-agnostic models [4, 24, 26, 27, 34, 37, 38] achieve impressive results and largely extend the applicability of models to heterogeneous clinical acquisition protocols. However, these models are only applicable to the tasks they were trained for.

Meanwhile, task-agnostic foundation models in computer vision and natural language processing have witnessed remarkable success, along with the fast developments of large-scale datasets [9, 13, 32]. Designed in a task-agnostic manner, foundation models have shown impressive performance in obtaining more general feature representations and can be quickly adapted (e.g., fine-tuned) to a wide range of downstream tasks [2, 6]. However, due to different acquisition protocols, processing pipelines, and privacy requirements across institutions, large-scale datasets in medical imaging require significantly more effort than natural imaging/language. As a result, medical foundation models are not as well developed. The MONAI [10] project includes a model zoo containing pre-trained models for various tasks, yet they are all highly task-oriented and sensitive to specific image contrasts. Zhou et al. [63] constructed a medical foundation model, yet it is designed for the detection of eye and systemic health conditions from retinal scans, and only works on the modalities of color fundus photography and optical coherence tomography. Lately, generalist biomedical AI systems [42, 48, 52] have shown great potential in biomedical tasks under vision-language context, e.g., (visual) question answering, image classification, radiology report generation and summarization. However, they have not explored the challenging vision tasks such as reconstruction, segmentation, super-resolution, and registration.

Here, we introduce **Brain-ID**, a subject-specific, contrast- and task-agnostic anatomical representation approach which is trained *entirely* on synthetic data, and can swiftly adapt to diverse downstream tasks through only *one* layer.

- 1) We introduce our on-the-fly, intra-subject data generator capable of synthesizing *any* contrast, employing a *mild-to-severe* increasing-corruption generation, all from the *same* brain anatomy (Fig. 2, Sec. 3.2). Unlike real-world datasets that are constrained by the images acquired per subject, **Brain-ID** learns in a much more expansive and diverse space.
- 2) We design a feature representation learning framework guided by the *unique anatomy* of each subject. Demonstrated by our proposed evaluation approach

for both inter- and intra-subject robustness, **Brain-ID**'s high-resolution features are consistently robust to the superficial perturbations of the input image's appearance (Sec. 4.2) such as contrast, resolution, orientation, artifacts. We further present straightforward one-layer adaptations that enable **Brain-ID** features to seamlessly adapt to downstream tasks (Sec. 3.3).

- 3) We extensively evaluate **Brain-ID** on both contrast-independent (anatomy reconstruction, brain segmentation) and contrast-dependent (super-resolution, bias field estimation) tasks, across six public datasets (around 8,000 images in total) including modalities of MR (T1w, T2w, FLAIR) and CT. **Brain-ID** achieves state-of-the-art performance in all tasks (Tab. 2). More importantly, it maintains its high performance even on low-resolution data (Fig. 6) and datasets with limited size (Fig. 7).

2 Related work

Feature Representation in Medical Imaging As discussed in Sec. 1, general feature representation learning in the medical imaging can be more challenging than in the natural image domain, due to limited data availability. Xu et al. [59] introduced a multiple instance learning model for feature representation in medical imaging, but it is designed specifically for classification, and only applies to histopathology images. You et al. [62] presented CVRL, a semi-supervised approach for voxel-wise representations, which is designed for image segmentation, but requires CT inputs to extract anatomical information. SAM [60] is a self-supervised framework to encode anatomical information from CT images for feature embeddings, which has shown to be effective in downstream tasks such as registration (SAMConvex [36]). However, same as CVRL, SAM only works on CT. BrainPrint [54] is a compact and discriminative representation of brain morphology, which is specifically designed for cortical surface analyses. To our best knowledge, CIFL [14] is the only existing work on learning contrast-agnostic and task-independent brain feature representations. CIFL relies on contrastive learning alone, and is insufficient to outperform task/contrast-specific supervised models in downstream applications as shown by our experiments (Tab. 2).

Contrast-invariant Learning for MR Images MRI scans acquired across sites vary substantially in contrasts, resolutions, orientations, etc. When given a new dataset, heterogeneity leads to duplicate training efforts for approaches that are sensitive to specific combinations of MR contrast, resolution, or orientation. Classical brain segmentation models used Bayesian inference for contrast-robustness [19, 35], which requires a long processing time and struggles with low or anisotropic resolutions [26, 44]. Recently, SynthSeg [4, 34] was proposed for contrast-agnostic segmentation and achieves impressive results with a synthetic generator that simulates widely diverse contrasts. Meanwhile, there have been works with similar ideas of using synthetic data to achieve contrast-invariance in tasks like image registration [24], super-resolution [27], and skullstripping [25]. However, all the above-mentioned methods are trained in a task-specific manner, whose features therefore cannot be readily applied to other domains.

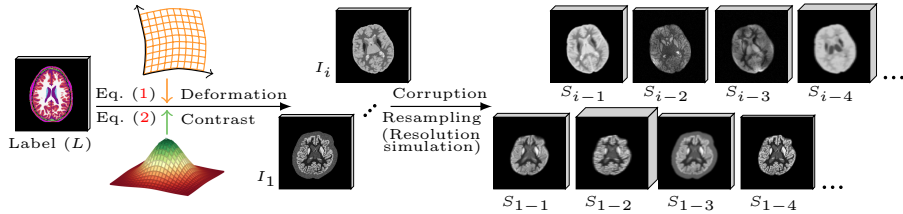


Fig. 2: Brain-ID’s data generator on the fly. Given the brain segmentation labels of a subject, we randomly generate a deformation field, and synthesize intra-subject samples featuring various contrast intensities and corruption levels (Sec. 3.1).

3 Brain-ID: Learning Anatomy-specific Brain Features

As discussed in Sec. 1, the main challenges to obtain a general and robust feature representation for MR imaging lie in (i) the practical restrictions of building large-scale datasets with diverse contrasts; and (ii) the nature of most medical imaging models that are task-oriented and specific to data type (contrast, resolution, orientation, etc). We aim to learn a brain feature representation that is:

(i) *Robust*: features should be robust to each subject’s distinct anatomy, unaffected by variations in poses/deformations, contrasts, resolutions, or artifacts.

(ii) *Expressive*: features should also exhibit high expressiveness, containing rich information that facilitates easy and effective adaptation to diverse downstream tasks, eliminating the necessity for extensive training data.

We first introduce Brain-ID’s data generator (Sec. 3.1) and training framework (Sec. 3.2) to achieve the above two aims. Then, we present our one-layer solutions for adapting Brain-ID features to downstream tasks that could be either dependent or independent of the contrast of input images (Sec. 3.3).

3.1 Enrich the Intra-subject Learning Space

A good representation relies on large-scale data, however, different acquisition protocols, processing pipelines, and privacy requirements across institutions make large-scale data less accessible and require significantly more effort, e.g., via federated learning [1, 16, 46]. Moreover, for each subject, there are usually only limited acquired images/modalities available. This lack of data consistency is a significant barrier to obtaining an subject-specific, contrast-invariant feature representation. Brain-ID avoids these barriers through the use of synthetic data.

In order to generate images with complex brain structures, we start from high-resolution brain segmentation images that provide labels of brain structures and extracerebral regions (L in Fig. 2). The generation consists of three steps, (i) deformation generation, (ii) contrast synthesis, and (iii) data corruption (including lower resolution resampling). For simplicity, Θ denotes the parameter group of the generation process described below.

Deformation Generation We first generate a random deformation field ($\phi|_{\theta_\phi}$) consisting of an affine transformation and a non-linear displacement field:

$$\phi|_{\theta_\phi} = \mathcal{T}|_{\theta_\phi} \circ \mathcal{A}|_{\theta_\phi}, \quad (1)$$

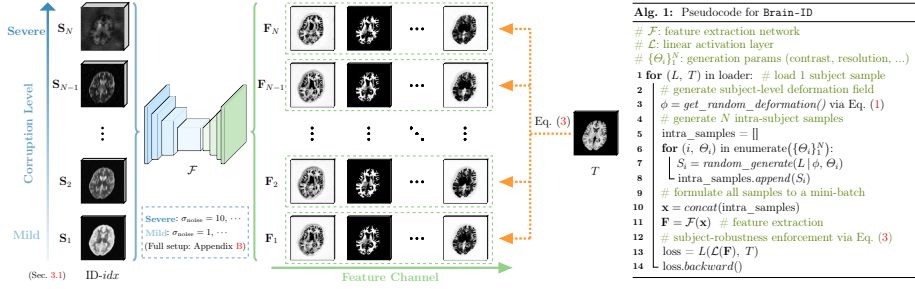


Fig. 3: Brain-ID’s contrast-agnostic anatomical representation learning framework.

where $\mathcal{A}|_{\theta_\phi}$ denotes an affine transformation matrix which includes linear (rotation, scaling, shearing) transformation and translation, $\mathcal{T}|_{\theta_\phi}$ refers to a non-linear displacement field computed as the integration of a stationary velocity field (SVF) that is smooth and invertible everywhere and thus preserves the topology of the brain anatomy [27]. $\theta_\phi \in \Theta$ controls the transformation ranges.

MR Contrast Synthesis Then, we synthesize images ($I(x), x \in \Omega$) by randomly “painting” intensities on the segmentation maps according to their brain structure labels ($l \in L$). Specifically, the regional intensities are generated by separately sampling a Gaussian distribution on each labeled region:

$$\begin{cases} I(x) \sim \mathcal{N}(\mu_l, \sigma_l), & l \in L, \\ \mu_l \sim \mathcal{N}(0, 1 | \theta_\mu, \theta_l), & \sigma_l \sim \mathcal{N}(0, 1 | \theta_\sigma, \theta_l), \end{cases} \quad (2)$$

where μ_l and σ_l refer to the mean and standard deviation of each segmentation label l , and are independently sampled from Gaussian distributions at each voxel, with $\theta_l, \theta_\mu, \theta_\sigma \in \Theta$ controlling the shifts and scales of their values.

Resolution Simulation and Data Corruption Given a deformed, contrast-synthesized image (I), we adopt the standard data corruption pipeline [26], which further augments images with different levels of resolution and scanning artifacts that are commonly found in real-world clinical protocols.

As illustrated in Fig. 2, we are able to generate an infinite number of variations from a single subject with its unique brain anatomy labels. By generating images with randomized contrast/resolution/orientation on the fly for each subject, we enormously enrich the learning space for a robust representation, and focus the learning on intrinsic subject-specific features rather than superficial aspects of images that depend on acquisition parameters and conditions. (In Sec. 4.5, we conduct experiments to provide insights on how different choices of data corruption levels would affect the robustness of Brain-ID features.)

3.2 Extract Robust and Expressive Subject-specific Features

As mentioned above, we would like the resulting features from Brain-ID to be both robust to intra-subject variations *and* expressive to potential downstream tasks. In this section, we introduce Brain-ID’s learning framework to achieve the two desired properties.

Intra-subject Data Generation In order to learn a feature representation that is distinctive to each subject and robust to varying MR contrasts, we observe that enriching *intra*-subject samples leads to better performance (Tab. 3). Specifically, instead of including multiple subjects for a mini-batch during each training iteration as in usual practice, **Brain-ID** focuses on maximizing the intra-subject variance to improve the subject-robustness of resulting features. As described in Alg. 1 (line 4-10), for each training iteration, after randomly selecting a subject and generating its deformation, **Brain-ID** generates a mini-batch of intra-subject samples ($\{S_1, \dots, S_N\}$) with randomly synthesized contrasts, resolutions and corruptions (Sec. 3.1). As will be introduced below, **Brain-ID** collects losses from all intra-subject samples and conducts back-propagation *at once*, to encourage the subject-specific robustness of its learned features.

We set the intra-subject samples within a mini-batch to have random contrasts and “mild-to-severe”, *increasing* level of corruptions (Fig. 3 (left)), to maximize the intra-subject variance while ensuring the stability of the training process against extreme corruption levels. (In Sec. 4.5, we compare various data generation designs, and provide insights on preventing unstable training.)

Anatomy-guided Feature Representation A richer learning space helps improve the representation robustness against the variance of sample appearances, but not enough for extracting expressive features. For example, a mapping that projects all inputs to zero is perfectly robust, but it does not provide any useful information for potential downstream tasks. Therefore, proper guidance is crucial for feature representation as well. In CIFL [14], the authors use a contrastive loss on feature channels to encourage a more discriminative feature representation. However, this method is insufficient, given the extremely complex nature of the human brain anatomy (See comparisons in Sec. 4). Instead, we propose to use the standard T1w high-resolution structural MR contrast for brain morphometry, i.e., MP-RAGE (magnetization-prepared rapid gradient-echo), as the unique anatomy target to guide **Brain-ID**’s feature representation learning.

As shown in Fig. 3, a feature extraction backbone (\mathcal{F}) first maps the input mini-batch of intra-subject generated samples, $\{S_1, \dots, S_N\}$, to their corresponding feature space, $\{\mathbf{F}_1, \dots, \mathbf{F}_N\}$. An linear activation layer (\mathcal{L}) then projects the features to the current subject’s standard contrast (MP-RAGE) space, T . The training loss is obtained by summing over the anatomy reconstruction loss of all intra-subject samples in the current mini-batch:

$$L = \sum_i^N |\mathcal{L}(\mathbf{F}_i) - T| + \lambda |\nabla \mathcal{L}(\mathbf{F}_i) - \nabla T|, \lambda \in R^+, \quad (3)$$

where T , as the high-resolution, unique anatomy target for all intra-subject samples, encourages the *similarities* of the features extracted from the same subject via reconstruction (1st term) and gradient difference (2nd term) L1 loss. **Brain-ID** uses MP-RAGE as the learning target, which formulates both super-resolution and contrast-synthesis problems, and encourages a richer feature representation. (Sec. 4.5 provides further insights on how different choices of anatomy guidance would affect the resulting features’ properties.)

3.3 Adapting Brain-ID to Downstream Tasks by One Layer

With the intra-subject data generation and anatomy-guided feature learning design introduced in Sec. 3.2, a well-trained **Brain-ID** model is able to extract robust, high-resolution anatomical features from images with varying deformations, contrasts, resolutions, and artifacts. To minimize the modifications, we propose straightforward *one-layer* solutions adapting **Brain-ID** features to various brain imaging applications. We later demonstrate that the simple adaptations are effective enough for **Brain-ID** to achieve state-of-the-art performance across all downstream tasks (Sec. 4.3), even for small datasets (Sec. 4.4).

Contrast-independent Tasks For tasks where the output should be independent of the input MR contrast, e.g., brain segmentation, we simply add an additional layer following **Brain-ID** features (\mathbf{F}), and fine-tune the model:

$$L = \text{task_loss_func}(\mathcal{L}(\mathbf{F}), T), \quad (4)$$

where \mathcal{L} and T refer to the task-specific activation layer and the contrast-independent ground truth, respectively.

Contrast-dependent Tasks Since **Brain-ID** features are contrast-agnostic and robust to artifacts, for tasks relevant to the input’s contrast/quality, e.g., super-resolution, we concatenate the input image (I) that contains the original contrast information with its high-resolution **Brain-ID** features along the channel dimension, before forwarding into the task-specific activation layer:

$$L = \text{task_loss_func}(\mathcal{L}(\mathbf{F} \oplus I), T), \quad (5)$$

where \mathcal{L} and T refer to the task-specific activation layer and the contrast-dependent ground truth, respectively.

4 Experiments

In this section, we conduct experiments to demonstrate the two properties of **Brain-ID** as claimed in Sec. 3. (i) Robustness (Sec. 4.2), where we propose “canonical” and “atlas-registered” features to assess both intra- and inter-subject robustness of **Brain-ID** features; (ii) Expressiveness (Sec. 4.3), where we evaluate the performance of adapting **Brain-ID** features to a series of common brain imaging applications. We further challenge **Brain-ID** with reduced-size datasets to explore its ability when limited real data is available for training (Sec. 4.4).

4.1 Datasets, Metrics and Implementation Details

Datasets For **Brain-ID** features pre-training, we use 2045 3D segmentations (“anatomies”, or IDs) from the public ADNI dataset [29]. For downstream evaluation, we use six public datasets covering T1w and T2w MRI, FLAIR MRI, and CT: ADNI [29], ADNI3 [58], HCP [18], ADHD200 [8], AIBL [22], OASIS3 [33].

Metrics We evaluate individual tasks from different aspects. For feature similarity measurements, we use L1 distance, and (MS-)SSIM (multi-scale structural similarity) [39, 56, 57]. For reconstruction and super-resolution, we use L1, PSNR (peak signal-to-noise ratio) and (MS-)SSIM. For segmentation, we use Dice scores. For bias field estimation, we use the normalized L2 distance (norm-L2) to avoid possible arbitrary scalings from nonuniformity correction [15]. (Appendix A contains further details on metrics and datasets preprocessing.)

Table 1: Evaluations on intra/inter-subject feature robustness.

Mode	Method	L1 (\downarrow)	SSIM (\uparrow)	MS-SSIM (\uparrow)
Intra	CIFL [14]	0.122 (± 0.031)	0.511 (± 0.298)	0.531 (± 0.367)
	Brain-ID	0.011 (± 0.001)	0.858 (± 0.041)	0.921 (± 0.008)
Inter	CIFL [14]	0.230 (± 0.039)	0.552 (± 0.240)	0.524 (± 0.291)
	Brain-ID	0.014 (± 0.013)	0.843 (± 0.044)	0.913 (± 0.011)

Implementation Details As a general feature representation model, **Brain-ID** can use any backbone to extract brain features. For fairer comparison, we adopt the same five-level 3D UNet [45] (with 64 feature channels in the last layer) as utilized in state-of-the-art models we compare with in Sec. 4.3. During feature pre-training (Sec. 3.2), a linear regression layer is added for anatomy supervision (Eq. (3)). For downstream adaptations, a task-specific adaption layer is added (Sec. 3.3). (More implementation details and training recipes are in Appendix B.)

4.2 Intra/Inter-subject Feature Robustness

In this section, we examine the robustness of **Brain-ID** features, i.e., the 64 features from the last layer. For comparable and reproducible results, we use our data generator (Sec. 3.1) to prepare (deform and corrupt) 1000 testing samples from 100 randomly selected subjects in ADNI [29] (T1w) testing set, with 10 intra-subject samples for each subject. (More details are in Appendix C.)

We compare our features with CIFL [14] which is, to our best knowledge, the only similar work to **Brain-ID**, that also aims to learn contrast-agnostic brain features. Note the original CIFL method has only experimented on 2D images, and does not have our intra-subject data generation design. For a fairer comparison, we trained CIFL *with its own contrastive-learning design*, while using the same data generator and network architecture as **Brain-ID**.

Intra-subject Feature Robustness Ideally, **Brain-ID** features computed from the same subject should be structurally *identical*, regardless of their appearances (contrast, resolution, noises, etc). To assess the intra-subject feature robustness, we first define their corresponding ‘‘canonical’’ features.

‘‘Canonical’’ Features. We compute ϕ^{-1} , the inverse of S ’ generated deformation as in Eq. (1), and map back each sample’s (S) **Brain-ID** features ($\mathbf{F} = \mathbf{F}(S | \phi)$) to their original domain without any deformation:

$$\mathbf{F}^{-1} = \phi^{-1} \circ \mathbf{F}(S | \phi). \quad (6)$$

As shown in Fig. 4(a), for the same subject (ID- i), although the inputs (row) are processed by varying deformations and corruptions, their **Brain-ID**’s ‘‘canonical’’ features are of similar looking along each feature channel (column). In Tab. 1, we quantify the feature similarity: For each testing subject, we first generate a sample *without* any deformation or corruption and use its **Brain-ID** feature as the gold-standard reference for all other ‘‘canonical’’ features computed from intra-subject samples that may have different levels of deformation and corruptions. The final results are obtained by scores averaged over all 64 feature channels of all the intra-subject samples.

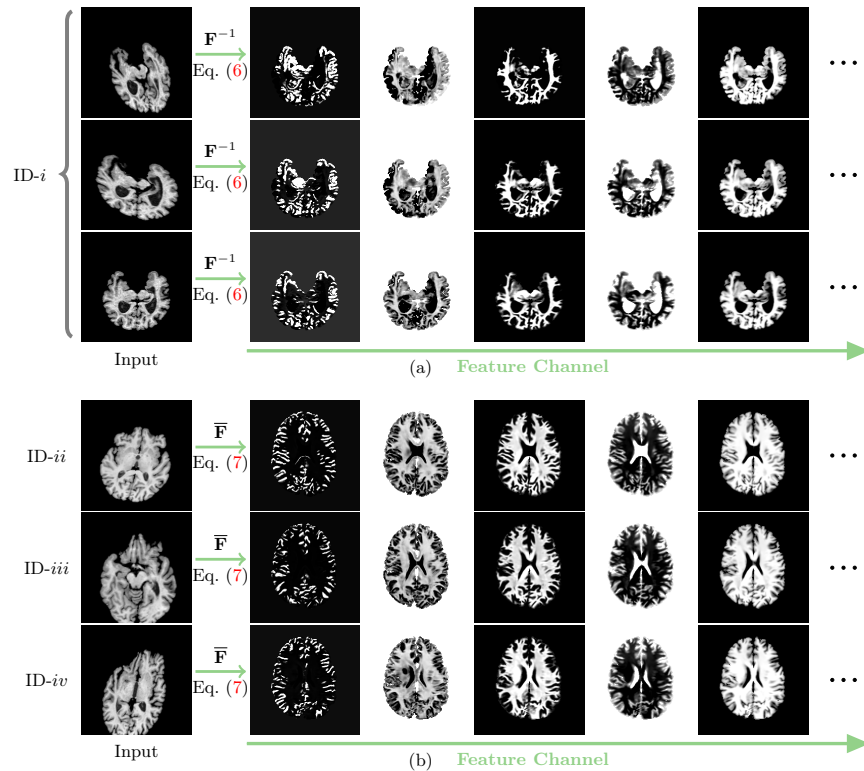


Fig. 4: (a) Intra-subject and (b) inter-subject robustness of Brain-ID features.

Inter-subject Feature Robustness We further assess the feature robustness among anatomies, based on the assumption that features from different subjects should ideally be *structurally similar*, once being registered to a common domain. “Atlas-registered” Features. We register [41] features ($\mathbf{F} = \mathbf{F}(S|\phi)$) from all subjects to a common brain atlas [20, 21]:

$$\bar{\mathbf{F}} = \psi_{S \rightarrow A} \circ \mathbf{F}(S|\phi), \quad (7)$$

where $\psi_{S \rightarrow A}$ denotes the mapping from S to the atlas, A .

As shown in Fig. 4(b), even though the input samples (row) from different subjects have varying anatomical structures, after being registered to a common domain, their “atlas-registered” Brain-ID features still appear consistent (column). In Tab. 1, we further provide quantitative results of the structural similarity measured between features from different subjects. Similar to Sec. 4.2, we randomly select a testing subject and generate a sample *without* any deformation or corruption. We use its “atlas-registered” Brain-ID feature as the gold standard for all “atlas-registered” features computed from other samples that may have different levels of deformation and corruption. The final results are obtained by scores averaged over all samples of the 100 testing subjects.

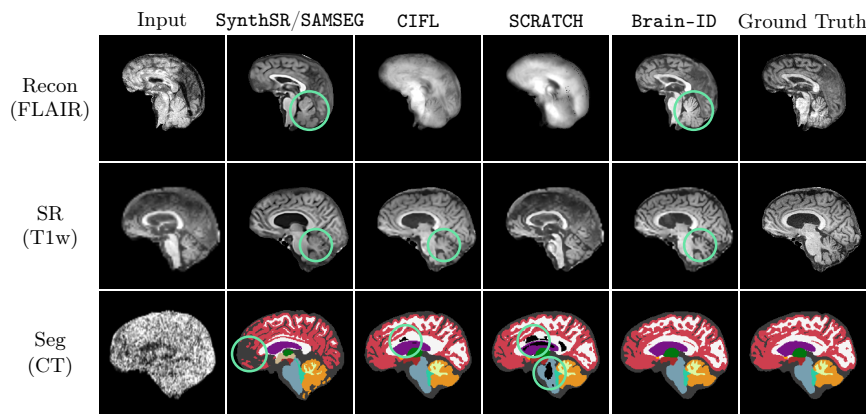


Fig. 5: Qualitative comparisons on downstream tasks of reconstruction (Recon), super-resolution (SR), and segmentation (Seg), between **Brain-ID**, the baseline **SCRATCH**, and the state-of-the-art methods **CIFL** [14], **SynthSR** [26] (Recon and SR), **SAMSEG** [12] (Seg). The visualized testing examples are taken from: AIBL-FLAIR [22] for Recon, AIBL-T1w [22] for SR, and OASIS-CT [33] for Seg. The **mint** circles highlight some details.

In both intra/inter-subject aspects, **Brain-ID** outperforms **CIFL** by a large margin, which validates its feature robustness against deformations, contrasts, resolutions, artifacts (intra-subject), and anatomies (inter-subject).

4.3 Downstream Evaluation

Following the standard evaluation protocol for feature representation learning [11], we fine-tune **Brain-ID** features for downstream tasks by the proposed one-layer adaption (Sec. 3.3). (More setup details and results are in Appendix D.)

Models We compare the downstream performance of **Brain-ID** features with: (i-ii) **SAMSEG** [12,44] and **FastSurfer** [23] (only works on T1w), state-of-the-art classical and machine-learning-based brain segmentation models, respectively; (iii) **SynthSR** [26], state-of-the-art, contrast-agnostic T1w synthesis model. We also provide fine-tuned **SynthSR** (**SynthSR-FT**) results for further comparison; (iv) **SCRATCH**: a baseline with the same data generation/architecture as **Brain-ID**, yet trained from *scratch*. **SCRATCH** is used to validate **Brain-ID**'s effectiveness. (v) **CIFL** [14]: a baseline with the same data generation/architecture as **Brain-ID** and **SCRATCH**, yet initialized with **CIFL**'s pre-trained features. We use **CIFL** to demonstrate the superiority of **Brain-ID**'s anatomy-guided representation.

Contrast-independent Applications

- Anatomy Reconstruction/Contrast Synthesis As one of the most common types of MRI scans, T1w MR images highlight the differences between gray and white matter, and are mostly often utilized to image the anatomy of the brain, spinal cord, bones and joints [49]. For each dataset, we train models to reconstruct their T1w MRI counterparts with the L1 loss.

Table 2: Comparisons of Brain-ID with state-of-the-art approaches on downstream applications. (“train/test” refers to the number of subjects in the training/testing set.)

Modality (Contrast)	Dataset (Train/Test)	Method	Reconstruction			Segmentation	Super-resolution (from 3 / 5 / 7 mm)			Bias Field	
			L1 (↓)	PSNR (↑)	SSIM (↑)	MS-SSIM (↑)	Dice (↑)	PSNR (↑)	SSIM (↑)	MS-SSIM (↑)	norm-L2 (↓)
MR (T1w)	ADNI [20] (1841/204)	SAMSEG [12]	-	-	-	-	-	-	-	-	-
		FastSurfer [23]	-	-	-	-	-	-	-	-	-
		SynthSR [26]	0.014	26.78	0.980	0.980	-	27.01 / 25.81 / 21.79	0.977 / 0.943 / 0.857	0.981 / 0.968 / 0.869	-
		SynthSR-FT	0.010	29.54	0.984	0.920	0.825	30.46 / 28.03 / 23.91	0.979 / 0.960 / 0.898	0.985 / 0.973 / 0.900	0.051
		CIFL [14]	0.013	26.97	0.973	0.961	0.820	30.12 / 27.21 / 23.80	0.978 / 0.912 / 0.887	0.979 / 0.950 / 0.842	0.053
		SCRATCH	0.011	27.34	0.979	0.957	0.816	30.29 / 27.34 / 24.57	0.975 / 0.959 / 0.920	0.982 / 0.964 / 0.866	0.056
	Brain-ID	0.012	33.82	0.993	0.989	0.837	31.30 / 28.62 / 24.68	0.983 / 0.961 / 0.928	0.987 / 0.980 / 0.947	0.048	
	HCP [18] (808/87)	SAMSEG [12]	-	-	-	-	-	-	-	-	-
		FastSurfer [23]	-	-	-	-	-	-	-	-	-
		SynthSR [26]	0.033	22.13	0.854	0.901	-	22.21 / 20.83 / 19.93	0.848 / 0.802 / 0.747	0.899 / 0.864 / 0.789	-
		SynthSR-FT	0.025	27.11	0.935	0.917	0.810	25.90 / 25.45 / 25.10	0.889 / 0.872 / 0.831	0.919 / 0.911 / 0.889	0.052
		CIFL [14]	0.029	26.42	0.932	0.913	0.804	25.98 / 25.11 / 23.99	0.930 / 0.883 / 0.871	0.936 / 0.927 / 0.880	0.059
SCRATCH		0.023	27.32	0.923	0.909	0.792	26.69 / 26.41 / 25.05	0.932 / 0.896 / 0.848	0.942 / 0.930 / 0.892	0.069	
Brain-ID	0.020	27.47	0.957	0.929	0.843	29.70 / 27.90 / 26.12	0.957 / 0.901 / 0.883	0.973 / 0.938 / 0.890	0.047		
MR (T2w)	ADNI9 [58] (298/33)	SAMSEG [12]	-	-	-	-	-	-	-	-	-
		FastSurfer [23]	-	-	-	-	-	-	-	-	-
		SynthSR [26]	0.023	23.60	0.928	0.909	-	23.13 / 22.40 / 22.27	0.921 / 0.907 / 0.876	0.903 / 0.892 / 0.871	-
		SynthSR-FT	0.021	27.11	0.950	0.969	0.820	27.95 / 27.34 / 26.18	0.920 / 0.913 / 0.890	0.922 / 0.890 / 0.879	0.134
		CIFL [14]	0.028	28.52	0.961	0.970	0.819	27.81 / 27.10 / 26.32	0.900 / 0.877 / 0.864	0.812 / 0.793 / 0.769	0.102
		SCRATCH	0.033	27.28	0.957	0.963	0.816	27.99 / 27.37 / 26.63	0.893 / 0.889 / 0.876	0.794 / 0.785 / 0.753	0.128
Brain-ID	0.021	29.89	0.966	0.976	0.843	30.17 / 28.23 / 26.89	0.962 / 0.923 / 0.892	0.973 / 0.945 / 0.883	0.093		
ADHD200 [8] (865/96)	SAMSEG [12]	-	-	-	-	-	-	-	-	-	
	FastSurfer [23]	-	-	-	-	-	-	-	-	-	
	SynthSR [26]	0.035	21.67	0.882	0.853	-	21.42 / 21.13 / 21.41	0.876 / 0.846 / 0.809	0.851 / 0.831 / 0.805	-	
	SynthSR-FT	0.016	26.90	0.917	0.905	0.812	28.55 / 27.43 / 25.94	0.880 / 0.859 / 0.823	0.860 / 0.845 / 0.811	0.110	
	CIFL [14]	0.013	28.69	0.932	0.921	0.810	28.11 / 26.12 / 25.11	0.865 / 0.848 / 0.831	0.828 / 0.800 / 0.789	0.109	
	SCRATCH	0.011	31.55	0.986	0.985	0.796	29.41 / 27.89 / 26.58	0.858 / 0.847 / 0.814	0.853 / 0.845 / 0.827	0.113	
Brain-ID	0.011	32.48	0.996	0.996	0.847	29.50 / 28.56 / 26.87	0.898 / 0.862 / 0.811	0.892 / 0.875 / 0.856	0.107		
AIBL [22] (601/67)	SAMSEG [12]	-	-	-	-	-	-	-	-	-	
	FastSurfer [23]	-	-	-	-	-	-	-	-	-	
	SynthSR [26]	0.026	22.95	0.916	0.912	-	22.57 / 21.82 / 21.78	0.917 / 0.892 / 0.856	0.906 / 0.893 / 0.869	-	
	SynthSR-FT	0.014	29.89	0.941	0.922	0.810	29.15 / 27.89 / 26.77	0.932 / 0.906 / 0.878	0.927 / 0.900 / 0.871	0.118	
	CIFL [14]	0.011	30.12	0.938	0.925	0.816	29.46 / 27.97 / 26.73	0.907 / 0.889 / 0.870	0.891 / 0.872 / 0.857	0.094	
	SCRATCH	0.011	30.53	0.932	0.913	0.814	29.43 / 28.10 / 26.82	0.900 / 0.886 / 0.863	0.884 / 0.870 / 0.853	0.128	
Brain-ID	0.009	33.73	0.972	0.963	0.851	29.75 / 28.58 / 27.09	0.957 / 0.922 / 0.890	0.975 / 0.956 / 0.937	0.088		
MR (T2w)	HCP [18] (808/87)	SAMSEG [12]	-	-	-	-	-	-	-	-	-
		SynthSR [26]	0.034	21.46	0.833	0.885	-	-	-	-	-
		SynthSR-FT	0.028	26.10	0.894	0.898	0.755	28.43 / 25.36 / 22.10	0.942 / 0.851 / 0.801	0.977 / 0.892 / 0.798	0.140
		CIFL [14]	0.036	25.12	0.891	0.879	0.787	28.26 / 25.78 / 21.73	0.959 / 0.893 / 0.797	0.982 / 0.906 / 0.742	0.138
		SCRATCH	0.038	24.99	0.873	0.866	0.756	28.12 / 24.52 / 21.58	0.945 / 0.863 / 0.783	0.980 / 0.893 / 0.738	0.136
		Brain-ID	0.016	28.10	0.934	0.935	0.805	30.26 / 26.11 / 24.10	0.959 / 0.902 / 0.832	0.987 / 0.953 / 0.912	0.136
MR (FLAIR)	AIBL [22] (272/30)	SAMSEG [12]	-	-	-	-	-	-	-	-	-
		SynthSR [26]	0.033	20.08	0.805	0.831	-	-	-	-	-
		SynthSR-FT	0.024	22.93	0.815	0.840	0.719	30.15 / 28.09 / 26.92	0.940 / 0.912 / 0.893	0.966 / 0.948 / 0.922	0.200
		CIFL [14]	0.022	23.71	0.820	0.839	0.721	29.98 / 27.01 / 25.66	0.931 / 0.899 / 0.861	0.967 / 0.941 / 0.905	0.193
		SCRATCH	0.020	22.27	0.849	0.851	0.714	31.91 / 29.20 / 27.35	0.954 / 0.934 / 0.896	0.982 / 0.969 / 0.947	0.197
		Brain-ID	0.022	23.99	0.861	0.850	0.782	32.26 / 29.90 / 27.09	0.973 / 0.937 / 0.900	0.988 / 0.971 / 0.948	0.148
MR (FLAIR)	ADNI9 [58] (298/33)	SAMSEG [12]	-	-	-	-	-	-	-	-	-
		SynthSR [26]	0.026	22.77	0.919	0.895	-	-	-	-	-
		SynthSR-FT	0.021	22.34	0.921	0.900	0.753	30.11 / 28.70 / 25.32	0.930 / 0.899 / 0.864	0.948 / 0.910 / 0.878	0.251
		CIFL [14]	0.020	21.29	0.911	0.897	0.761	32.72 / 29.00 / 26.99	0.949 / 0.906 / 0.873	0.953 / 0.919 / 0.889	0.237
		SCRATCH	0.025	20.80	0.901	0.862	0.759	32.36 / 28.71 / 28.00	0.945 / 0.915 / 0.877	0.941 / 0.936 / 0.917	0.236
		Brain-ID	0.017	26.44	0.927	0.892	0.786	32.18 / 30.00 / 28.28	0.959 / 0.921 / 0.883	0.982 / 0.965 / 0.921	0.227
MR (FLAIR)	AIBL [22] (302/34)	SAMSEG [12]	-	-	-	-	-	-	-	-	-
		SynthSR [26]	0.029	21.77	0.902	0.892	-	-	-	-	-
		SynthSR-FT	0.024	25.80	0.914	0.900	0.735	26.20 / 24.91 / 23.17	0.860 / 0.832 / 0.795	0.933 / 0.910 / 0.894	0.126
		CIFL [14]	0.026	27.11	0.901	0.870	0.721	27.72 / 26.85 / 25.99	0.851 / 0.828 / 0.804	0.939 / 0.905 / 0.901	0.109
		SCRATCH	0.023	26.84	0.898	0.867	0.730	28.02 / 26.52 / 25.43	0.878 / 0.838 / 0.799	0.943 / 0.901 / 0.891	0.115
		Brain-ID	0.019	27.25	0.936	0.912	0.787	28.69 / 27.63 / 26.69	0.949 / 0.906 / 0.866	0.971 / 0.925 / 0.916	0.103
MR (FLAIR)	OASIS3 [33] (795/88)	SAMSEG [12]	-	-	-	-	-	-	-	-	-
		SynthSR [26]	0.041	20.93	0.758	0.786	-	-	-	-	-
		SynthSR-FT	0.030	23.76	0.797	0.845	0.700	25.30 / 22.18 / 20.35	0.892 / 0.813 / 0.760	0.896 / 0.801 / 0.764	-
		CIFL [14]	0.027	24.91	0.819	0.871	0.718	25.99 / 23.70 / 22.83	0.909 / 0.820 / 0.779	0.969 / 0.816 / 0.775	-
		SCRATCH	0.025	24.35	0.811	0.872	0.709	26.34 / 23.64 / 22.62	0.905 / 0.818 / 0.770	0.873 / 0.818 / 0.780	-
		Brain-ID	0.023	25.49	0.891	0.895	0.765	26.74 / 24.01 / 23.09	0.910 / 0.818 / 0.792	0.974 / 0.824 / 0.799	-

(1) “-” means not applicable; FastSurfer [23] and SAMSEG [12] are for segmentation-only; SynthSR [26] only synthesizes T1w MRI; CT does not have bias fields.

(2) SynthSR-FT: SynthSR fine-tuned on each task/dataset, for a fairer comparison.

- **Brain Segmentation** For each dataset, we use SynthSeg [4] to obtain the segmentation labels with 30 brain anatomical regions [19], as the gold standard segmentation target. We train our compared models to predict the brain segmentation labels, with the soft dice loss and cross-entropy loss [4].

As shown in Fig. 5, Brain-ID clearly outperforms CIFL and SCRATCH in the reconstruction task. As highlighted by the mint circles, it reveals the anatomy details and produces more fine-grained results than the strong state-of-the-art method SynthSR [26]. Brain-ID also achieves better segmentation results, especially in the smaller and more challenging regions. Quantitative comparisons are in Tab. 2, where Brain-ID obtains the best scores across most metrics. Notably, Brain-ID achieves greater gains over baseline models, SCRATCH and CIFL,

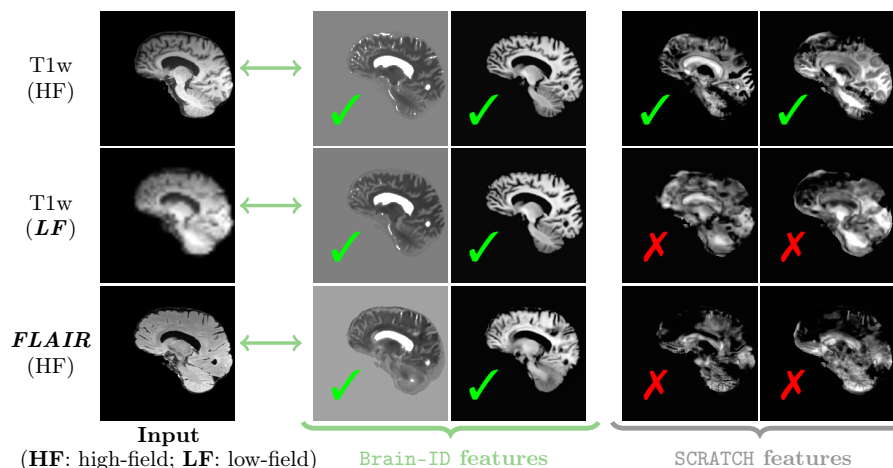


Fig. 6: SCRATCH, which is well trained on HF T1w scans, produces highly descriptive features for HF T1w images (1st row), but *does not preserve* the same high quality useful for downstream tasks when handling LF (2nd row) or other contrasts (3rd row).

particularly on smaller datasets (e.g., ADNI3-T1/FLAIR, AIBL-FLAIR, where Brain-ID’s robust and rich features quickly adapt to specific tasks/datasets.

Contrast-dependent Applications We also evaluate Brain-ID on two brain imaging tasks that are dependent on the input modality/quality.

- **Image Super-resolution** We use the standard $1mm$ isotropic images from all datasets as the ground truth high-resolution target, and follow the strategy in SynthSR [26] where the input samples are randomly resampled and corrupted during training. For inference, we downsample the original images into $3mm$, $5mm$, and $7mm$ isotropic images as inputs, and evaluate the output quality.

- **Bias Field Estimation** The bias field is a smooth, low-frequency multiplicative signal that corrupts MRI images, which affects image analysis tasks such as segmentation or texture analysis [30]. Bias field estimation is often needed as a pre-processing step to correct corrupted MRI images [15]. We apply randomly simulated bias fields to the input samples (Sec. 3.1), and train all models with the L2 loss. During inference, we pre-generate and apply the bias fields on the testing data for reproducibility, and evaluate the bias field estimation performance.

With a simple one-layer adaption (Sec. 3.3), Brain-ID’s contrast-agnostic anatomical features achieve state-of-the-art performance on contrast-dependent tasks (Tab. 2, Fig. 5). As shown in Fig. 6, Brain-ID obtains contrast/resolution-robustness that *cannot* be achieved by models trained from real images (due to the *limited variability* in their appearance), regardless of the backbone choices. Such robust features greatly improve super-resolution, resulting in higher (MS-)SSIM scores. Brain-ID’s gains are less obvious for bias field estimation, probably due to the fact that the bias field is approximately *independent* of brain anatomy.

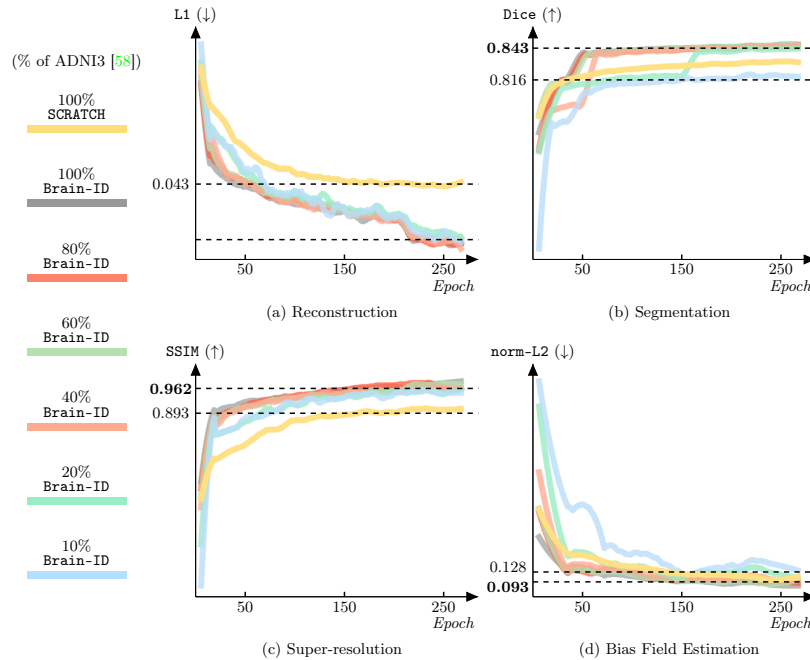


Fig. 7: Adapting **Brain-ID** to small datasets. The horizontal (vertical) axes indicate training epochs (evaluation scores of corresponding tasks). Results are obtained by evaluating models collected throughout the epochs, on ADNI3 [58] full testing set.

4.4 Practical Value and Broader Impact

Low-resolution data Trained on synthetic images, **Brain-ID** features are not only robust to various contrasts/modalities, but also extremely robust to low-resolution data (Fig. 6) and provide huge potential in clinical MRI (including big retrospective data [5]) and portable low-field MRI [28].

Small-size Datasets To investigate the effectiveness of **Brain-ID** features for limited-size datasets, we assess its performance across all four downstream tasks on subsets of ADNI3 [58] training set (298 cases originally). As shown in Fig. 7, we reduce the training set size percentage from 100% to an extreme 10%. With only 20% of the data (mint line), **Brain-ID** still achieves better performance compared to its full-sized baseline, “100%” **SCRATCH** (yellow line), over all tasks. 30 training samples (10%, blue line) may be at the edge of obtaining acceptable results for **Brain-ID**, as the model becomes less stable and the performance drops occur more frequently – especially for brain segmentation (Fig. 7-(b)).

4.5 Additional Experiments and Further Discussions

Choice of Anatomy Guidance We explore other anatomical learning targets than MP-RAGE (Sec. 3.2): (i) segmentation labels; (ii) both segmentation labels and MP-RAGE. As shown in Tab. 3, adding segmentation guidance improves

Table 3: Comparison between **Brain-ID** and its variants.

Model Setup [Comparison Target]	Feature Robustness (Intra)		Downstream (Reconstruction)		
	SSIM (\uparrow)	MS-SSIM (\uparrow)	L1 (\downarrow)	PSNR (\uparrow)	SSIM (\uparrow)
<i>[Representation guidance: supervision target for feature learning]</i>					
Segmentation	0.891	0.963	0.029	28.13	0.958
Segmentation + MP-RAGE	0.863	0.940	0.023	29.05	0.964
MP-RAGE (Brain-ID)	0.858	0.921	0.021	29.89	0.966
<i>[Data generation design: corruption levels in intra-subject mini-batches]</i>					
All Mild ($\sigma_{\text{noise}} = 1, \dots$)	0.792	0.813	0.028	28.30	0.960
All Medium ($\sigma_{\text{noise}} = 5, \dots$)	0.831	0.899	0.022	29.67	0.964
All Severe ($\sigma_{\text{noise}} = 10, \dots$)	N/A	N/A	N/A	N/A	N/A
Mild to Severe (Brain-ID)	0.858	0.921	0.021	29.89	0.966
<i>[Mini-batch size: number of intra-subject samples]</i>					
2	0.826	0.897	0.025	28.83	0.959
3	0.841	0.902	0.022	29.30	0.962
4 (Brain-ID)	0.858	0.921	0.021	29.89	0.966
5	0.860	0.929	0.021	29.93	0.965

robustness, yet inhibits the feature expressiveness and affects the downstream performance; we observe features obtained from segmentation guidance produce less high-frequency texture than **Brain-ID**, especially *within* the same-label regions. (Please refer to the visualizations in Fig. E.1, Appendix E.)

Data Generation Design As shown in Tab. 3, training with all mildly-corrupted samples results in reduced feature robustness and further harms the downstream performance, yet using all extremely corrupted samples leads to unstable training and model collapse. We train **Brain-ID** on samples of gradually increased corruptions (Fig. 3 (left)). (Appendix B lists the full parameter setups.)

Batch Size **Brain-ID** computes training loss of all intra-subject samples in a mini-batch at once (Eq. (3)). We observe that larger batches help improve feature robustness (Tab. 3), yet do not further enhance the downstream performance.

Limitations **Brain-ID** is designed to capture the unique anatomy of subjects, it works exceptionally well on fundamental brain imaging tasks such as reconstruction, segmentation, and super-resolution, with a simple one-layer adaption. However, as **Brain-ID**'s data generation is solely based on anatomies, we observe that it is not adept at handling images with extensive pathology regions. Our future work will focus on contrast-agnostic, pathology-encoded representations.

5 Conclusion

We introduced **Brain-ID**, a contrast-agnostic anatomical representation learning approach for brain imaging, which is distinctive to each subject's anatomy and resilient to variations in image appearances. **Brain-ID** is trained entirely on synthetic data, and quickly and effectively adapts to downstream tasks through only a single layer. We validated **Brain-ID** features' intra/inter-subject robustness, and effectiveness on four downstream applications (reconstruction, segmentation, super-resolution, bias field estimation). Experiments on six public datasets, covering MR and CT, demonstrated that **Brain-ID** achieves state-of-the-art performance across all tasks and modalities, and preserves high performance on low-resolution data and small-size datasets. We believe **Brain-ID** unlocks the great potential of robust foundation models, especially for non-calibrated modalities.

References

1. Adnan, M., Kalra, S., Cresswell, J.C., Taylor, G.W., Tizhoosh, H.R.: Federated learning and differential privacy for medical image analysis. *Scientific reports* (2022) [4](#)
2. Awais, M., Naseer, M., Khan, S.S., Anwer, R.M., Cholakkal, H., Shah, M., et al.: Foundational models defining a new era in vision: A survey and outlook. *arXiv abs/2307.13721* (2023) [2](#)
3. Balakrishnan, G., Zhao, A., Sabuncu, M.R., Guttag, J.V., Dalca, A.V.: VoxelMorph: A learning framework for deformable medical image registration. *IEEE Transactions on Medical Imaging* (2018) [2](#)
4. Billot, B., Greve, D.N., Puonti, O., Thielscher, A., Leemput, K.V., Fischl, B.R., et al.: SynthSeg: Segmentation of brain MRI scans of any contrast and resolution without retraining. *Medical Image Analysis* (2021) [2](#), [3](#), [11](#), [19](#)
5. Billot, B., Magdamo, C., Cheng, Y., Arnold, S.E., Das, S., Iglesias, J.E.: Robust machine learning segmentation for large-scale analysis of heterogeneous clinical brain MRI datasets. *Proceedings of the National Academy of Sciences* (2023) [13](#)
6. Bommasani, R., Hudson, D.A., Adeli, E., Altman, R., Arora, S., von Arx, S., et al.: On the opportunities and risks of foundation models. *arXiv abs/2108.07258* (2021) [2](#)
7. Brant-Zawadzki, M.N., Gillan, G.D., Nitz, W.R.: MP RAGE: A three-dimensional, T1-weighted, gradient-echo sequence—initial experience in the brain. *Radiology* (1992) [2](#)
8. Brown, M.R.G., Sidhu, G.P.S., Greiner, R., Asgarian, N., Bastani, M., Silverstone, P.H., et al.: ADHD-200 global competition: diagnosing ADHD using personal characteristic data can outperform resting state fMRI measurements. *Frontiers in Systems Neuroscience* (2012) [7](#), [11](#), [19](#)
9. Brown, T., Mann, B., Ryder, N., Subbiah, M., Kaplan, J.D., Dhariwal, P., et al.: Language models are few-shot learners. In: *NeurIPS* (2020) [2](#)
10. Cardoso, M.J., Li, W., Brown, R., Ma, N., Kerfoot, E., Wang, Y., et al.: MONAI: An open-source framework for deep learning in healthcare. *arXiv abs/2211.02701* (2022) [2](#)
11. Caron, M., Touvron, H., Misra, I., Jégou, H., Mairal, J., Bojanowski, P., Joulin, A.: Emerging properties in self-supervised vision transformers. In: *ICCV* (2021) [10](#)
12. Cerri, S., Puonti, O., Meier, D.S., Wuerfel, J., Mühlau, M., Siebner, H.R., Leemput, K.V.: A contrast-adaptive method for simultaneous whole-brain and lesion segmentation in multiple sclerosis. *NeuroImage* (2020) [10](#), [11](#), [22](#), [26](#)
13. Chowdhery, A., Narang, S., Devlin, J., Bosma, M., Mishra, G., Roberts, A., et al.: PaLM: Scaling language modeling with pathways. *JMLR* (2022) [2](#)
14. Chua, Y.Z.R., Dalca, A.V.: Contrast invariant feature representations for segmentation and registration of medical images. In: *MIDL* (2023) [3](#), [6](#), [8](#), [10](#), [11](#), [24](#), [25](#), [26](#)
15. Chua, Z.Y., Zheng, W., Chee, M.W.L., Zagorodnov, V.: Evaluation of performance metrics for bias field correction in MR brain images. *Journal of Magnetic Resonance Imaging* (2009) [7](#), [12](#), [19](#)
16. Darzidehkalani, E., Ghasemi-Rad, M., van Ooijen, P.: Federated learning in medical imaging: Part I: Toward multicentral health care ecosystems. *Journal of the American College of Radiology* (2022) [4](#)
17. Ding, Z., Han, X., Liu, P., Niethammer, M.: Local temperature scaling for probability calibration. In: *ICCV* (2021) [2](#)

18. Essen, D.C.V., Ugurbil, K., Auerbach, E.J., Barch, D.M., Behrens, T.E.J., Bucholz, R.D., et al.: The human connectome project: A data acquisition perspective. *NeuroImage* (2012) [7](#), [11](#), [19](#)
19. Fischl, B.R., Salat, D.H., Busa, E., Albert, M.S., Dieterich, M., Haselgrove, C., et al.: Whole brain segmentation automated labeling of neuroanatomical structures in the human brain. *Neuron* (2002) [3](#), [11](#)
20. Fonov, V.S., Evans, A.C., Botteron, K., Almli, C.R., McKinstry, R.C., Collins, D.L., et al.: Unbiased average age-appropriate atlases for pediatric studies. *Neuroimage* (2011) [9](#)
21. Fonov, V.S., Evans, A.C., McKinstry, R.C., Almli, C.R., Collins, D.: Unbiased nonlinear average age-appropriate brain templates from birth to adulthood. *NeuroImage* (2009) [9](#)
22. Fowler, C., Rainey-Smith, S.R., Bird, S., Bomke, J., Bourgeat, P., Brown, B.M., et al.: Fifteen years of the australian imaging, biomarkers and lifestyle (AIBL) study: Progress and observations from 2,359 older adults spanning the spectrum from cognitive normality to Alzheimer’s disease. *Journal of Alzheimer’s disease reports* (2021) [7](#), [10](#), [11](#), [19](#)
23. Henschel, L., Conjeti, S., Estrada, S., Diers, K., Fischl, B.R., Reuter, M.: FastSurfer - A fast and accurate deep learning based neuroimaging pipeline. *NeuroImage* (2019) [10](#), [11](#), [22](#)
24. Hoffmann, M., Billot, B., Greve, D.N., Iglesias, J.E., Fischl, B.R., Dalca, A.V.: SynthMorph: Learning contrast-invariant registration without acquired images. *IEEE Transactions on Medical Imaging* (2020) [2](#), [3](#)
25. Hoopes, A., Mora, J.S., Dalca, A.V., Fischl, B.R., Hoffmann, M.: SynthStrip: skull-stripping for any brain image. *NeuroImage* (2022) [3](#), [19](#)
26. Iglesias, J.E., Billot, B., Balbastre, Y., Magdamo, C.G., Arnold, S., Das, S., et al.: SynthSR: A public AI tool to turn heterogeneous clinical brain scans into high-resolution T1-weighted images for 3D morphometry. *Science Advances* (2023) [2](#), [3](#), [5](#), [10](#), [11](#), [12](#), [22](#), [24](#), [25](#)
27. Iglesias, J.E., Billot, B., Balbastre, Y., Tabari, A., Conklin, J., Alexander, D.C., et al.: Joint super-resolution and synthesis of 1 mm isotropic MP-RAGE volumes from clinical MRI exams with scans of different orientation, resolution and contrast. *NeuroImage* (2020) [2](#), [3](#), [5](#)
28. Iglesias, J.E., Schleicher, R., Laguna, S., Billot, B., Schaefer, P., McKaig, B., et al.: Quantitative brain morphometry of portable low-field-strength MRI using super-resolution machine learning. *Radiology* (2022) [13](#)
29. Jack, C.R., Bernstein, M.A., Fox, N.C., Thompson, P.M., Alexander, G.E., Harvey, D.J., et al.: The Alzheimer’s disease neuroimaging initiative (ADNI): MRI methods. *Journal of Magnetic Resonance Imaging* (2008) [7](#), [8](#), [11](#), [18](#), [19](#), [21](#)
30. Juntu, J., Sijbers, J., Dyck, D.V., Gielen, J.: Bias field correction for MRI images. In: *CORES* (2005) [12](#)
31. Kamnitsas, K., Ledig, C., Newcombe, V.F.J., Simpson, J.P., Kane, A.D., Menon, D.K., et al.: Efficient multi-scale 3D CNN with fully connected CRF for accurate brain lesion segmentation. *Medical Image Analysis* (2016) [2](#)
32. Kirillov, A., Mintun, E., Ravi, N., Mao, H., Rolland, C., Gustafson, L., et al.: Segment anything. *arXiv abs/2304.02643* (2023) [2](#)
33. LaMontagne, P.J., Keefe, S.J., Lauren, W., Xiong, C., Grant, E.A., Moulder, K.L., et al.: OASIS-3: Longitudinal neuroimaging, clinical, and cognitive dataset for normal aging and Alzheimer’s disease. *Alzheimer’s & Dementia* (2018) [7](#), [10](#), [11](#), [19](#)

34. Laso, P., Cerri, S., Sorby-Adams, A., Guo, J., Mateen, F., Goebel, P., et al.: Quantifying white matter hyperintensity and brain volumes in heterogeneous clinical and low-field portable MRI. arXiv [abs/2312.05119](#) (2023) [2](#), [3](#)
35. Leemput, K.V., Maes, F., Vandermeulen, D., Suetens, P.: A unifying framework for partial volume segmentation of brain MR images. *IEEE Transactions on Medical Imaging* (2003) [3](#)
36. Li, Z., Tian, L., Mok, T.C.W., Bai, X., Wang, P., Ge, J., et al.: SAMConvex: Fast discrete optimization for CT registration using self-supervised anatomical embedding and correlation pyramid. In: *MICCAI* (2023) [3](#)
37. Liu, P., Lee, Y., Aylward, S., Niethammer, M.: Deep decomposition for stochastic normal-abnormal transport. In: *CVPR* (2022) [2](#)
38. Liu, P., Tian, L., Zhang, Y., Aylward, S., Lee, Y., Niethammer, M.: Discovering hidden physics behind transport dynamics. In: *CVPR* (2021) [2](#)
39. Liu, P., Wang, R., Cao, X., Zhou, Y., Shah, A., Lim, S.N.: Differential motion evolution for fine-grained motion deformation in unsupervised image animation. arXiv [abs/2110.04658](#) (2021) [7](#), [20](#)
40. Milletari, F., Navab, N., Ahmadi, S.A.: V-Net: Fully convolutional neural networks for volumetric medical image segmentation. *3DV* (2016) [2](#)
41. Modat, M., Ridgway, G.R., Taylor, Z.A., Lehmann, M., Barnes, J., Hawkes, D.J., et al.: Fast free-form deformation using graphics processing units. *Computer Methods and Programs in Biomedicine* (2010) [9](#), [19](#)
42. Moor, M., Banerjee, O., Abad, Z.F.H., Krumholz, H.M., Leskovec, J., Topol, E.J., Rajpurkar, P.: Foundation models for generalist medical artificial intelligence. *Nature* (2023) [2](#)
43. Müller, R.A., Shih, P., Keehn, B., Deyoe, J.R., Leyden, K.M., Shukla, D.: Under-connected, but how? A survey of functional connectivity MRI studies in autism spectrum disorders. *Cerebral Cortex* (2011) [2](#)
44. Puonti, O., Iglesias, J.E., Leemput, K.V.: Fast and sequence-adaptive whole-brain segmentation using parametric bayesian modeling. *NeuroImage* (2016) [3](#), [10](#), [22](#)
45. Ronneberger, O., Fischer, P., Brox, T.: U-Net: Convolutional networks for biomedical image segmentation. In: *MICCAI* (2015) [2](#), [8](#), [20](#)
46. Sheller, M.J., Edwards, B., Reina, G.A., Martin, J., Pati, S., Kotrotsou, A., et al.: Federated learning in medicine: Facilitating multi-institutional collaborations without sharing patient data. *Scientific reports* (2020) [4](#)
47. Shen, Z., Feydy, J., Liu, P., Curiale, A.H., San Jose Estepar, R., San Jose Estepar, R., Niethammer, M.: Accurate point cloud registration with robust optimal transport. In: *NeurIPS* (2021) [2](#)
48. Singhal, K., Azizi, S., Tu, T., Mahdavi, S., Wei, J., Chung, H.W., et al.: Large language models encode clinical knowledge. *Nature* (2022) [2](#)
49. Symms, M.R., Jäger, H.R., Schmierer, K., Yousry, T.A.: A review of structural magnetic resonance neuroimaging. *Journal of Neurology, Neurosurgery & Psychiatry* (2004) [10](#)
50. Tanno, R., Worrall, D.E., Kaden, E., Alexander, D.C.: Uncertainty modelling in deep learning for safer neuroimage enhancement: Demonstration in diffusion MRI. *NeuroImage* (2020) [2](#)
51. Tian, Q., Bilgiç, B., Fan, Q., Ngamsombat, C., Zaretskaya, N., Fultz, N.E., et al.: Improving in vivo human cerebral cortical surface reconstruction using data-driven super-resolution. *Cerebral Cortex* (2020) [2](#)
52. Tu, T., Azizi, S., Driess, D., Schaekermann, M., Amin, M., Chang, P.C., et al.: Towards generalist biomedical AI. arXiv [abs/2307.14334](#) (2023) [2](#)

53. de Vos, B.D., Berendsen, F.F., Viergever, M.A., Sokooti, H., Staring, M., Išgum, I.: A deep learning framework for unsupervised affine and deformable image registration. *Medical Image Analysis* (2019) [2](#)
54. Wachinger, C., Golland, P., Reuter, M.: BrainPrint: Identifying subjects by their brain. In: *MICCAI* (2014) [3](#)
55. Wang, M., Deng, W.: Deep visual domain adaptation: A survey. *Neurocomputing* (2018) [2](#)
56. Wang, T.C., Mallya, A., Liu, M.Y.: One-shot free-view neural talking-head synthesis for video conferencing. In: *CVPR* (2021) [7](#), [20](#)
57. Wang, Z., Simoncelli, E.P., Bovik, A.C.: Multiscale structural similarity for image quality assessment. In: *ACSSC* (2003) [7](#), [20](#)
58. Weiner, M.W., Veitch, D.P., Aisen, P.S., Beckett, L.A., Cairns, N.J., Green, R.C., et al.: The Alzheimer’s disease neuroimaging initiative 3: Continued innovation for clinical trial improvement. *Alzheimer’s & Dementia* (2017) [7](#), [11](#), [13](#), [19](#)
59. Xu, Y., Mo, T., Feng, Q., Zhong, P., Lai, M., Chang, E.I.C.: Deep learning of feature representation with multiple instance learning for medical image analysis. In: *ICASSP* (2014) [3](#)
60. Yan, K., Cai, J., Jin, D., Miao, S., Harrison, A.P., Guo, D., et al.: SAM: Self-supervised learning of pixel-wise anatomical embeddings in radiological images. *IEEE Transactions on Medical Imaging* (2020) [3](#)
61. Yang, X., Kwitt, R., Niethammer, M.: Quicksilver: Fast predictive image registration – a deep learning approach. *NeuroImage* (2017) [2](#)
62. You, C., Zhao, R., Staib, L.H., Duncan, J.S.: Momentum contrastive voxel-wise representation learning for semi-supervised volumetric medical image segmentation. In: *MICCAI* (2021) [3](#)
63. Zhou, Y., Chia, M.A., Wagner, S.K., Ayhan, M.S., Williamson, D.J., Struyven, R.R., et al.: A foundation model for generalizable disease detection from retinal images. *Nature* (2023) [2](#)

Appendix for Brain-ID

A Datasets and Metrics

Datasets We test and compare our method over various datasets including modalities of MR and CT, the MR images further contain T1-weighted, T2-weighted and FLAIR (fluid-attenuated inversion recovery) images.

- ADNI [\[29\]](#): we use T1-weighted (2045 cases) MRI scans from the Alzheimer’s Disease Neuroimaging Initiative (ADNI). All scans are acquired at 1 *mm* isotropic resolution from a wide array of scanners and protocols. The dataset contains aging subjects, some diagnosed with mild cognitive impairment (MCI) or Alzheimer’s Disease (AD). Many subjects present strong atrophy patterns and white matter lesions.

- HCP [18]: we use T1-weighted (897 cases) and T2-weighted (897 cases) MRI scans of young subjects from the Human Connectome Project, acquired at 0.7 mm resolution.
- ADNI3 [58]: we use T1-weighted (331 cases) and FLAIR (331 cases) MRI scans from ADNI3, which continues the previously funded ADNI1, ADNI-GO, and ADNI2 studies to determine the relationships between the clinical, cognitive, imaging, genetic and biochemical biomarker characteristics of the entire spectrum of sporadic late onset AD.
- ADHD200 [8]: we use T1-weighted (961 cases) MRI scans from ADHD200 Sample, which is a grassroots initiative dedicated to the understanding of the neural basis of Attention Deficit Hyperactivity Disorder (ADHD).
- AIBL [22]: we use T1-weighted (668 cases), T2-weighted (302 cases) and FLAIR (336 cases) MRI scans from The Australian Imaging, Biomarkers and Lifestyle (AIBL) Study, which is a study of cognitive impairment (MCI) and Alzheimer’s disease dementia.
- OASIS3 [33]: we use CT (885 cases) scans from OASIS3, which is a longitudinal neuroimaging, clinical, and cognitive dataset for normal aging and AD. For our experiments, we use CT and T1-weighted MRI pair with the earliest date, from each subject.

Data for Synthetic Generator Brain-ID’s synthetic generator uses (1) brain segmentation labels, for random-contrast input images generation (Sec. 3.1), and (2) MP-RAGE, the target ground truth for anatomy-guided supervision (Sec. 3.2). In this work, we use the segmentation maps of training images from ADNI [29], as well as their corresponding MP-RAGE images. Note that we do not use any type of real images from ADNI as input for Brain-ID’s pre-training.

Data Preprocessing For all datasets, we skull-strip all the images using SynthStrip [25], and resample them to 1 mm isotropic resolution. For all the images, except T1-weighted MRI, in each dataset, we use NiftyReg [41] rigid registration to register all images to their same-subject T1-weighted MRI counterparts. The gold-standard brain segmentation maps are obtained by performing SynthSeg [4] on the T1-weighted MR images of all the subjects.

Metrics We resort to various metrics for evaluating individual tasks across multiple aspects:

- L1: the average $L1$ distance, is used for intra/inter-subject feature distance evaluation (Sec. 4.2), and the overall prediction correctness of anatomy reconstruction (Sec. 4.3), super-resolution and bias-field estimation (Sec. 4.3).
- normL2: the normalized $L2$ distance for bias field [15] is defined as:

$$\text{normL2} = \sqrt{\frac{\sum_x (wB_{\text{est}}(x) - B_{\text{true}}(x))^2}{\sum_x B_{\text{true}}^2(x)}}, \quad (\text{A.1})$$

where w is the normalization coefficient obtained by:

$$w = \frac{\sum_x B_{\text{true}}(x)B_{\text{est}}(x)}{\sum_x B_{\text{est}}^2(x)}, \quad x \in \Omega, \quad (\text{A.2})$$

Ω refers to the brain domain, B_{est} and B_{true} are the estimated and ground truth bias fields, respectively. Normalization is necessary for the evaluation of bias field estimation (Sec. 4.3) because nonuniformity correction may result in arbitrary scaling of the bias field.

- PSNR: the peak signal-to-noise ratio (PSNR) that indicates the fidelity of predictions. It is used in anatomy reconstruction (Sec. 4.3) and super-resolution (Sec. 4.3).
- (MS-)SSIM: the structural similarity scores between the generated and real images. MS-SSIM is a variant of SSIM focusing on multiple scales of the images that are shown to correlate well with human perception [39, 56, 57]. They are used in intra/inter-subject feature distance evaluation (Sec. 4.2), reconstruction (Sec. 4.3), and super-resolution (Sec. 4.3),
- Dice: the similarity score between predicted and ground truth segmentations, and it is used in brain segmentation evaluation (Sec. 4.3).

B Implementation Details

Model Architecture As mentioned in Sec. 4, **Brain-ID** can use any backbone to extract brain features. We use the five-level 3D UNet [45] as **Brain-ID**’s backbone for feature extraction, with 64 feature channels in the last layer.

- During the feature pre-training stage (Sec. 3.2), a linear regression layer is added following the feature outputs for anatomy supervision (Eq. (3)).
- During downstream tasks adaptations, the regression layer for anatomy supervision is abandoned, instead, a task-specific activation layer is added following the feature outputs (Sec. 3.3). Specifically, a linear regression layer is added for the tasks, anatomy reconstruction/contrast synthesis, image super-resolution, and bias field estimation. An additional softmax activation is added for segmentation probability outputs.

Feature Backbone Pre-training We pre-train **Brain-ID** on the synthetic data from our generator (Sec. 3.1) for 300,000 iterations, with a patch size of 128^3 and a mini-batch size (i.e., number of intra-subject augmented samples) of 4. We use the synchronized AdamW optimization, with a base learning rate of 10^{-4} and a linear warm-up in the first 2,000 iterations followed by a multi-step learning schedule (learning rate drops at 160,000 and 240,000 iterations) with a multiplier of 0.1.

Synthetic Data Generator As shown in Fig. 3, **Brain-ID** simulates its training samples of increasing corruption levels, from mild to severe. Tab. 3 also

Table B.1: Brain-ID synthetic generator setups: mild, medium and severe levels. p denotes probability, μ and σ refer to the mean and variance of the Gaussian distributions, respectively.

Category	Param	Corruption Level		
		Mild	Medium	Severe
Deformation	affine-rotation _{max}	15	=	=
	affine-shearing _{max}	0.2	=	=
	affine-scaling _{max}	0.2	=	=
	nonlinear-scale μ_{min}	0.03	=	=
	nonlinear-scale μ_{max}	0.06	=	=
	nonlinear-scale σ_{max}	4	=	=
Resolution	$p_{low-field}$	0.1	0.3	0.5
	$p_{anisotropic}$	0	0.1	0.25
Bias Field	μ_{min}	0.01	0.02	0.02
	μ_{max}	0.02	0.03	0.04
	σ_{min}	0.01	0.05	0.1
	σ_{max}	0.05	0.3	0.6
Noises	σ_{min}	0.01	0.5	5
	σ_{max}	1	5	15

explores the effects of different levels of sample corruption on feature robustness and downstream performance. In Tab. B.1, we list the generator parameters for mild, medium, and severe data corruption levels, respectively. Note that (1) for each level, the setup parameters only control the corruption value ranges, since the simulation is randomized, there could still be mildly corrupted samples generated under the “severe” settings; (2) The random deformation fields are independent of data corruption levels.

C Feature Robustness Evaluation

For the evaluation of feature robustness, we use T1-weighted MRI of 100 randomly selected subjects from ADNI [29]. To challenge the model’s robustness against data corruptions, and meanwhile obtain comparable and reproducible results, we use our data generator (Sec. 3.1) to pre-augment all the input images. Note that in this section, there is no contrast simulation step within data augmentation, and only the random deformation and data corruptions are applied. For each selected subject, we generate intra-augmented samples. All samples are generated with “medium” corruption settings as listed in Tab. B.1.

D Downstream Task Comparisons

For all the downstream tasks, the model architecture and data generation strategy used for Brain-ID, SCRATCH and CIFL are the same. The only difference between the three compared models lies in their initial weights. Brain-ID and

CIFL are initialized by their pre-trained weights from training on synthetic data as described in Secs. 3.1 and 3.2.

For the state-of-the-art comparisons, we consider **FastSurfer** [23] and **SAMSEG** [12,44] for brain segmentation, and **SynthSR** [26] for anatomy reconstruction/contrast synthesis and super-resolution for T1-weighted images.

- **FastSurfer** [23] is a state-of-the-art brain segmentation model, which is designed for segmentation on T1-weighted images. Therefore, we only report the segmentation performance of **FastSurfer** on T1-weighted MRI. In addition, since **FastSurfer** does not predict cerebrospinal fluid (CSF), we remove the CSF label during the **Dice** score computation.
- **SAMSEG** [12,44] is a state-of-the-art, multi-modal brain segmentation model, which works on both MR and CT images. Similar to **FastSurfer**, **SAMSEG** does not predict the CSF label either, the CSF label is therefore removed during the **Dice** score computation of **SAMSEG**.
- **SynthSR** [26] is a state-of-the-art, contrast-agnostic model for anatomy reconstruction/contrast synthesis. For input MRI images with any contrast and resolution, **SynthSR** generates their corresponding high-resolution, 1 mm isotropic T1-weighted MRI. In our comparisons, we apply **SynthSR** on our anatomy reconstruction/contrast synthesis task, as well as the image super-resolution task of T1-weighted MRI.

E Additional Experimental Results

Feature Representation Learning As discussed in Sec. 4.5, in **Brain-ID** we adopt the high-resolution MP-RAGE scan as the anatomy guidance for brain feature representation. Experimental comparisons in Tab. 3 illustrate that incorporating segmentation as the target for anatomical supervision in learning brain feature representation leads to reduced high-frequency texture compared to the use of MP-RAGE alone. The visual comparisons presented in Fig. E.1 reveal that the features with segmentation guidance indeed encompass anatomical structures, however, they exhibit notably smoother texture *within* each structural region defined by the brain segmentation labels. In contrast, employing MP-RAGE as the target for anatomical supervision inherently entails the tasks of anatomy reconstruction and super-resolution simultaneously. The resulting features from **Brain-ID** are shown to carry richer information content, as evidenced by the more pronounced high-frequency textures they manifest.

Downstream Task Evaluation In addition to the qualitative results in Figs. 1 and 5, we provide more visualization comparisons of the downstream tasks in Figs. E.2 to E.4.

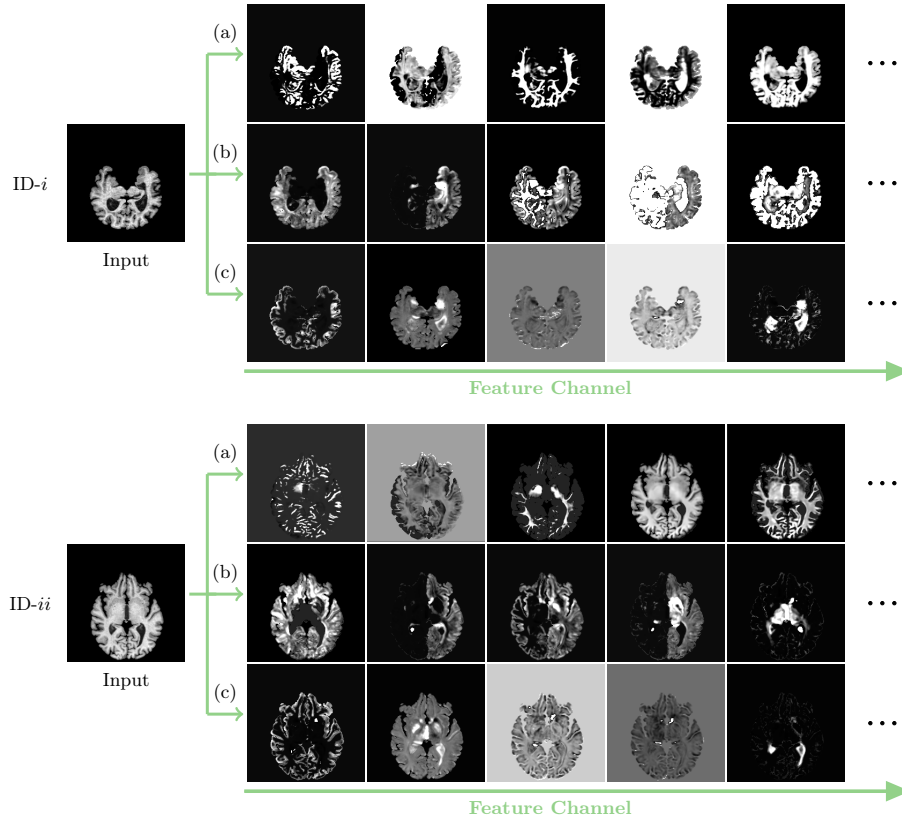


Fig. E.1: Visualization comparisons for features computed from (a) **Brain-ID** (MP-RAGE guided) with its variants: (b) segmentation guided and (c) segmentation + MP-RAGE guided feature representation models. Note that although the two testing subjects here for the three models are the same, their respective selected feature channels are different, for the purpose of better showing different frequency levels of features from each model.

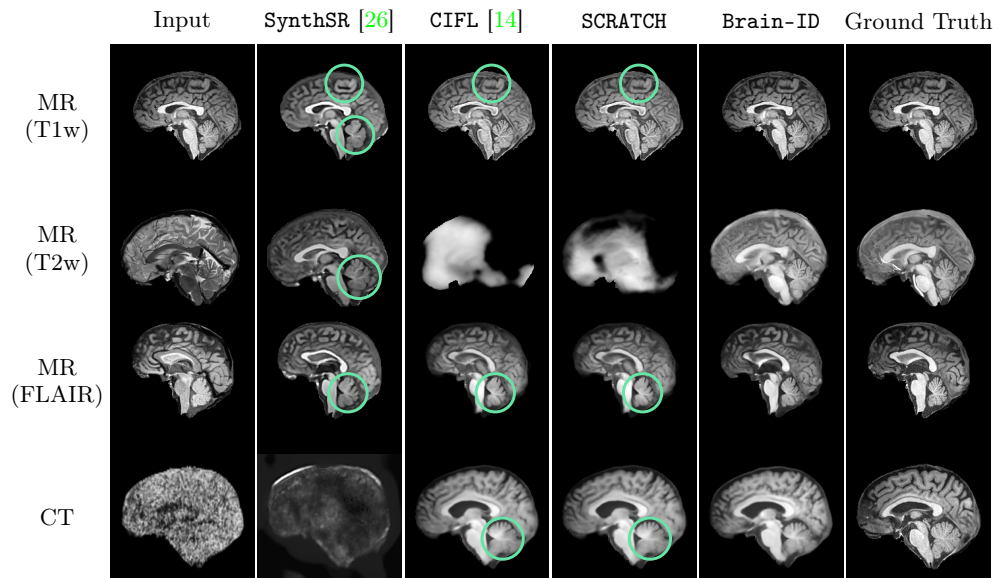


Fig. E.2: Qualitative comparisons on the downstream task of anatomy reconstruction/contrast synthesis, between **Brain-ID**, the baseline **SCRATCH**, and the state-of-the-art methods **CIFL** [14], **SynthSR** [26]. Each row presents the comparison results of inputs with their respective modality/contrast, as indicated in the listing. The **mint** circles highlight some less noticeable details.

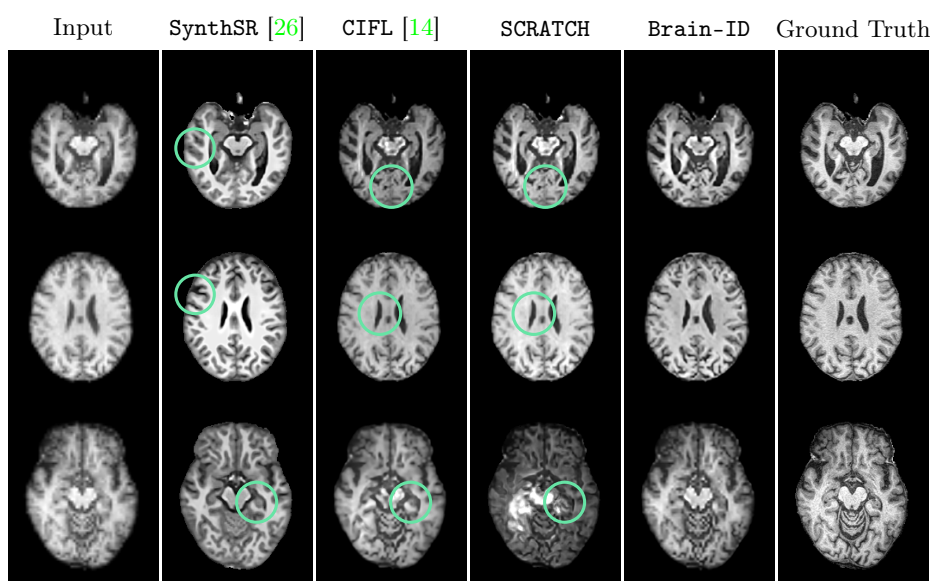


Fig. E.3: Qualitative comparisons on the downstream task of image super-resolution, between **Brain-ID**, the baseline **SCRATCH**, and the state-of-the-art methods **CIFL** [14], **SynthSR** [26]. Each row corresponds to a different testing subject. The **mint** circles highlight some less noticeable details.

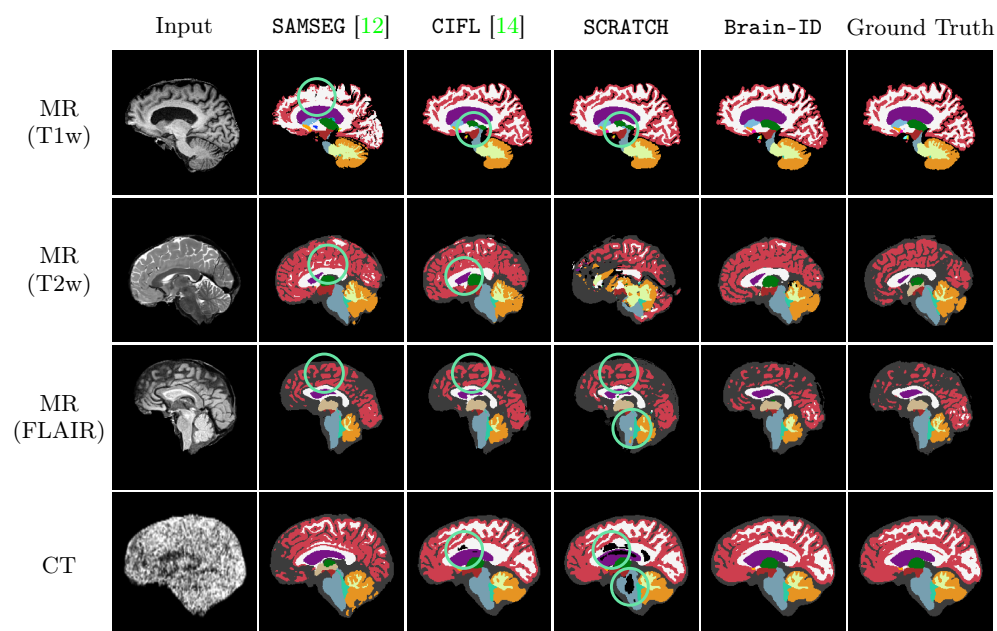


Fig.E.4: Qualitative comparisons on the downstream task of brain segmentation, between **Brain-ID**, the baseline **SCRATCH**, and the state-of-the-art methods **CIFL** [14], **SAMSEG** [12]. Each row presents the comparison results of inputs with their respective modality/contrast, as indicated in the listing. The **mint** circles highlight some less noticeable details.